V European Conference on Computational Fluid Dynamics
ECCOMAS CFD 2010
J. C. F. Pereira and A. Sequeira (Eds)
Lisbon, Portugal,14-17 June 2010

BUBBLE MODEL FOR CAVITATING FLOW SIMULATION INCLUDING HIGH VOID FRACTION REGION

Nobuo Tsurumi*, Yoshiaki Tamura† and Yoichiro Matsumoto††

*Intelligent Material and Mechatronics Systems, Toyo University
Kujirai 2100, Kawagoe, Saitama 350-8585, Japan
e-mail: tsurumi@cse.eng.toyo.ac.jp
†Information Sciences and Arts, Toyo University
Kujirai 2100, Kawagoe, Saitama 350-8585, Japan
e-mail: tamtam@eng.toyo.ac.jp
††Mechanical Engineering, The University of Tokyo
Hongo 7-3-1, Bunkyo-ku, Tokyo 113-8656, Japan
e-mail: ymats@mech.t.u-tokyo.ac.jp

Key words: Cavitation, Multiphase Flow, Cavitating Flow, Bubble Model, Rayleigh-Plesset equation

Abstract. *The present authors have been developing cavitating flow simulation method based on the dynamics of cavitation bubbles solving so-called Rayleigh-Plesset (R-P) equation to simulate precise motions of bubbles and pressure field around the bubbles. The advantage of bubble dynamics based model is that relative velocity of bubble can be considered, e. g., bubble accumulation can be simulated and that the pressure radiated from the collapsed bubble can be estimated. On the other hand, bubble dynamics based model tends to be stiff (hard to stably solve) and R-P equation is not valid in high void fraction region such as sheet cavitation because R-P equation assumes spherical bubble shape and no interaction between bubbles. In the present paper, a new bubble model valid for high void fraction region is proposed. Up to 90% of void fraction is stably simulated.*

1 INTRODUCTION

Cavitating flow simulation is still one of the challenging topics in CFD. There are some published works[1]–[3] but most of the works related to the cavitating flow simulation are limited within conference talks[4]–[8] and there is no definitive method in this field. Cavitating flow simulation methods are categorized into three groups. The first group is the method based on VOF[1],[2]. VOF based method is suitable for the case of rather large bubbles, e. g., sheet cavitations and bubble cavitations. Oppositely for the case of tiny bubbles whose size and slip velocity are to be negligible, barotropic model (or homogenization model) based method are applicable[4]–[7]. In this type of methods, the governing equation is for single phase flow with a special equation of state which models the thermodynamic state of mixture, including cavitation (vaporization and condensation). In between, there are bubble dynamics based methods[3],[8]. The advantage of bubble dynamics based model is that relative velocity of bubble can be considered, e. g., bubble accumulation can be simulated and that the pressure radiated from the collapsed bubble can be estimated and thus these methods could possibly be extended to erosion estimation[9]. On the other hand, the bubble dynamics based methods tend to be unstable in computation due to the stiffness of the governing equations and cannot allow high void fraction as most of the bubble dynamics model is based on the Rayleigh-Plesset equation which implies that bubble - bubble interactions are negligible. In the present paper, an extension of a bubble dynamics based method for higher void fraction region with sufficient stability and efficiency is described. The basic idea is to switch the Rayleigh-Plesset equation to another (rather simple) model of reasonable assumptions for higher void fraction region, where the liquid pressure is consequently low in general. In the following sections, the governing equations of the present method and the solution algorithm are described and the results of two-dimensional flow around a hydrofoil are presented to show the validity and the capability of the present method.

2 NUMERICAL METHOD

As temporal and spatial scale of cavitation bubble is much smaller than those of entire flow field, followings are assumed to obtain the governing equations[3].

- Liquid phase is incompressible, gas phase is compressible.
- Density and momentum of gas phase are sufficiently small compared to liquid phase.
- Gas phase consists of bubbles. All bubbles are spherical and no collision and coalescence occur.
- Mass change due to the phase change is much smaller than the mass of liquid.
- Bubbles are filled with vapor and non-condensable gas. The pressure inside a bubble is uniform. The vapor pressure is constant. The pressure of non-condensable gas is modeled to simulate vaporization and condensation at the interface.

Each bubble is assumed to follow Rayleigh-Plesset equation in rather low void fraction region, or, as far as it works. Otherwise another simple bubble growth model is applied to extend the present method for higher void fraction region.

2.1 Governing Equations

According to the assumptions, the following equations are derived. The dependent variables are number density, radius and velocity of bubbles and pressure and velocity of liquid phase.

1) Conservation of the number density of bubbles

$$\frac{\partial n_G}{\partial t} + J\frac{\partial \left(n_G U_{Gj}/J\right)}{\partial \xi_j} = 0 \tag{1}$$

n_G is the number density of bubbles. The Subscript G denotes the gas phase (L the liquid phase). This and the following equations are written in the generalized coordinate of ξ_i and U is contravariant velocity. J is the Jacobian.

2) Translational motion of a bubble

$$F_{Ii} + F_{Ai} + F_{Pi} + F_{Di} + F_{Li} + F_{Hi} = 0 \tag{2}$$

Here F_{Ii} is the inertia force of a bubble and F_{Hi} is the history force and both are neglected. F_{Ai} is the added mass force, F_{Pi} the force by the acceleration of the surrounding liquid, F_{Di} the drag force and F_{Li} the lift force and their details are found in [3].

3) Volumetric motion of a bubble (Rayleigh-Plesset equation)

$$r_G\frac{D^2 r_G}{Dt^2} + \frac{3}{2}\left(\frac{Dr_G}{Dt}\right)^2 = \frac{p_B - p_L}{\rho_L} + \frac{1}{4}\left|\vec{u}_G - \vec{u}_L\right|^2 \tag{3}$$

r_G is the radius of a bubble. p is a pressure, ρ is density and u is velocity in Cartesian coordinate. p_B is a pressure inside of a bubble and given as,

$$p_B = p_v + p_G - \frac{2T}{r_G} - 4\mu_L\frac{1}{r_G}\frac{Dr_G}{Dt} \tag{4}$$

T is the surface tension and p_v is the vapor pressure and both are constant in the present research. p_G is the pressure of non-condensable gas and modeled to simulate the single bubble motion as,

$$\begin{array}{l} p_G r_G^3 = const.\ (Dr_G/Dt > 0) \\ p_G r_G^{3\kappa} = const.\ (Dr_G/Dt < 0) \end{array} \tag{5}$$

κ is the specific heat ratio and taken to be 1.4. This is a simplified model from the observation of a very precise simulation[10] and was validated in [11].

4) Conservation of the volumetric fraction of liquid phase

$$\frac{\partial f_L}{\partial t} + J\frac{\partial \left(f_L U_{Lj}/J\right)}{\partial \xi_j} = 0 \tag{6}$$

f_L is the volume fraction of liquid. This is lead from the mass conservation of mixture with the assumption that the liquid is incompressible and the density of the gas is neglected.

5) Conservation of momentum

$$\frac{\partial \left(\rho_L f_L u_{Li}\right)}{\partial t} + J\frac{\partial \left(\rho_L f_L u_{Li} U_{Lj}/J\right)}{\partial \xi_j} = -\nabla_i p_L + \nabla_k \left(\mu \nabla_k u_{Li}\right) + \frac{1}{3}\left(\mu \nabla_k u_{Lk}\right) \tag{7}$$

Here the density of gas is neglected. μ is effective viscosity of bubbly flow and given as,

$$\mu = \left\{1 + f_G\left(\frac{\mu_L + 5/2\mu_G}{\mu_L + \mu_G}\right)\right\}\mu_L \cong \left(1 + f_G\right)\mu_L \tag{8}$$

f_G is the void fraction.

6) Constraint of volumetric fractions

$$f_G + f_L = 1 = \frac{4}{3}\pi r_G^3 n_G + f_L \tag{9}$$

This closes the system of equations.

2.2 Introduction of Pseudocompressibility

In order to obtain liquid pressure directly, pseudocompressibility is introduced[3]. Only the final form of equation is shown here.

$$\frac{1}{c^2}\frac{\partial p_L}{\partial t} + \nabla_i f_L u_{Li} + \nabla_i f_G u_{Gi} - 4\pi r_G^2 n_G \frac{Dr_G}{Dt} = 0 \tag{10}$$

where c^2 is pseudocompressibility constant. Equation (10) is then solved instead of Eq. (6) and f_L is obtained by Eq. (9).

2.3 Solution Algorithm

Firstly, Equation (2) is solved. The equation is convection - diffusion equation with source terms. The convection term is discretized with upwind difference, the viscous term with central difference. Implicit time integration of LU-SGS with sub-iterations is adopted. Secondly, Equation (3) is divided into four equations, namely,

$$\frac{\partial r_G}{\partial t} + U_{Gj}\frac{\partial r_G}{\partial \xi_j} = 0 \tag{3a}$$

$$\frac{\partial \dot{r}_G}{\partial t} + U_{Gj}\frac{\partial \dot{r}_G}{\partial \xi_j} = 0 \tag{3b}$$

$$r_G\frac{d^2 r_G}{dt^2} + \frac{3}{2}\left(\frac{dr_G}{dt}\right)^2 = \frac{p_B - p_L}{\rho_L} + \frac{1}{4}\left|\vec{u}_G - \vec{u}_L\right|^2 \tag{3c}$$

$$\frac{dr_G}{dt} = \dot{r}_G \tag{3d}$$

and Equations (3a) and (3b) are solved together with Eq. (1) as they are all convection equations with bubble velocity. They are discretized as the same as Eq. (2) described above. The division of Eq. (3) is expected to give more stability in the computation as well as smooth change of bubble dynamics model from Eq. (3c) for higher void fraction described later. Equations (3c) and (3d) are integrated by Runge - Kutta method with the modified equations of Eqs. (4) and (5) as,

$$p_B = p_v + p_G - \frac{2T}{r_G} - 4\mu_L\frac{\dot{r}_G}{r_G} \tag{4}'$$

$$\begin{array}{l} p_G r_G^3 = const.\ (\dot{r}_G > 0) \\ p_G r_G^{3\kappa} = const.\ (\dot{r}_G < 0) \end{array} \tag{5}'$$

Finally Equations (7) and (10) are solved as the same as the other convection - diffusion equations. The liquid fraction of f_L is then obtained with Eq. (9).

2.4 Cavitation Model

The present bubble dynamics model may break down where the local void fraction is large mainly because of the following reason. Let's consider the equilibrium state, namely, $\dot{r}_G = 0$ in Eq. (4)′. With a certain initial condition, void fraction of equilibrium state versus the liquid pressure is given as shown in Fig. 1. From the figure, we notice that void fraction very rapidly increases when the liquid pressure goes down below the vapor pressure. Because of this equilibrium curve, bubbles could hardly be settled around the vapor pressure and possibly diverge. The idea of the present bubble model is to swtich from Rayleigh-Plesset equation to another model before the bubbles diverge around the vapor pressure. The switching point might differ from the initial condition. In this paper we choose initial void fraction of 0.1% and initial bubble radius of 10μm to make the model. Figure 2 shows a bubble behavior in sudden pressure decrease down to just above 140Pa and Figure 3 just below 140Pa where the lateral axis is time (step), red line is the normalized bubble radius, blue the normalized liquid pressure and green the normalized pressure inside of the bubble. As clearly seen in these figures, the bubble suddenly breaks at a certain liquid pressure. When the bubble oscillates as in Fig. 2, the maximum bubble radius corresponds to the void fraction of 10 - 50%. Thus we adopt the void fraction of 30% as the switching point in this paper.

Two models are proposed here. Model 1 simply set the upper limit of void fraction to 30%. When the liquid pressure is below the vapor pressure and the local void fraction

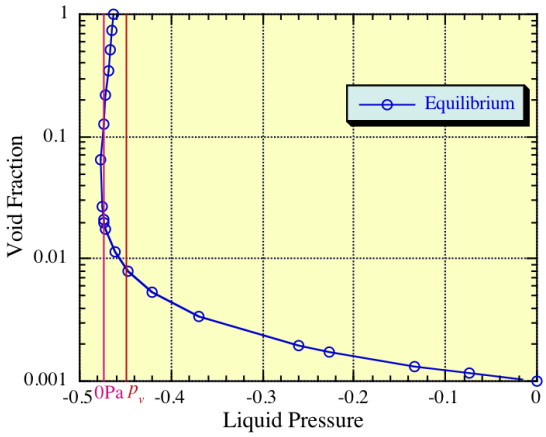

Figure 1: Liquid pressure versus void fraction (equilibrium state)

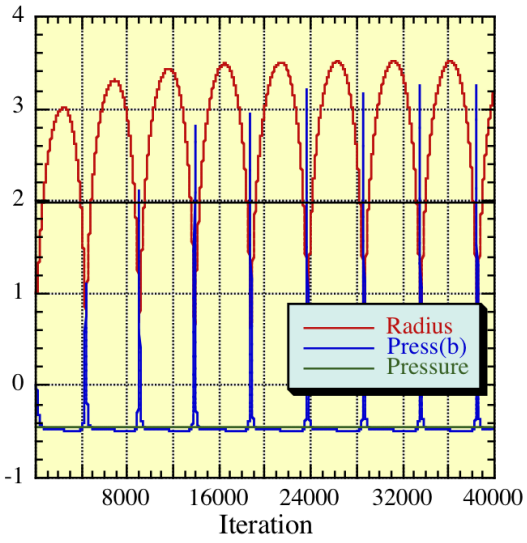

Figure 2: Bubble motion in sudden pressure decrease (oscillation)

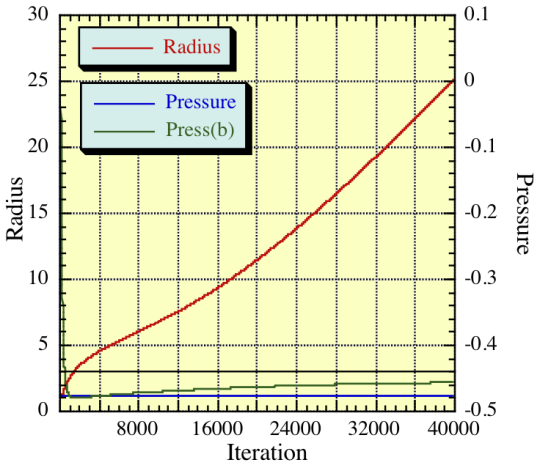

Figure 3: Bubble motion in sudden pressure decrease (divergence)

increases up to 30%, the bubble motion is frozen instead of solving Eq. (3c) and the liquid pressure is also set to be the vapor pressure. When the void fraction goes down below 30% after solving Eq. (3a) or the pressure recovers above the vapor pressure after solving Eq. (10), Rayleigh-Plesset equation again starts to be solved.

Model 2 is an extension of Model 1. Instead of freezing the bubble motion, $\dot{r}_G$ is frozen instead of solving Eq. (3c). The basis of the idea freezing $\dot{r}_G$ is that the bubble radius growth is almost linear in Fig. 3. When the void fraction reaches nearly 100% (90% is adopted in this paper), $\dot{r}_G$ is now set to be zero to stop expansion. When the liquid pressure recovers above the vapor pressure, Rayleigh-Plesset equation starts to be solved again just as Model 1.

In both models, slip velocity $(\vec{u}_G - \vec{u}_L)$ is set to be zero at and above the void fraction of 30% because the bubble translation model (Eq. (2)) is no more valid in such high void fraction.

3 NUMERICAL RESULTS

Two examples of flow around two-dimensional hydrofoils are presented here to show the validity of the present method.

3.1 Clark-Y 11.4%

The first example is flow around a hydrofoil of Clark-Y 11.4%. The conditions are summarized in Table 1. Figure 4 shows a close-up view of the computational grid. Flows

angles-of-attack	2.0°
chord length	0.1m
initial radius of bubble nucleus	10μm
initial void fraction	0.1%
uniform flow velocity	10m/s
Reynolds number	6×10^5
surface tension	$7.2\times\ 10^{-2}$N/m
vapor pressure	2.3×10^3Pa
number of grid points	281×41

Table 1: Conditions for Clark-Y 11.4%

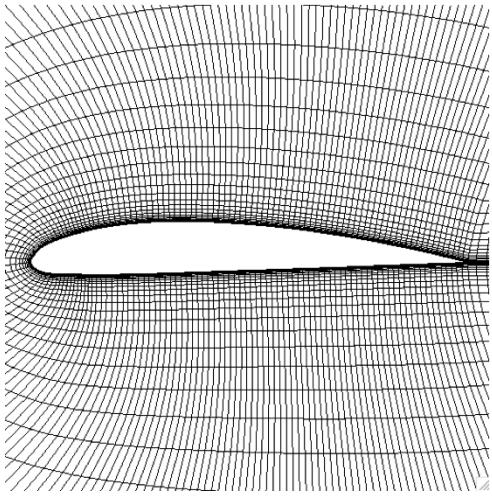

Figure 4: Computational grid for Clark-Y 11.4% (close-up)

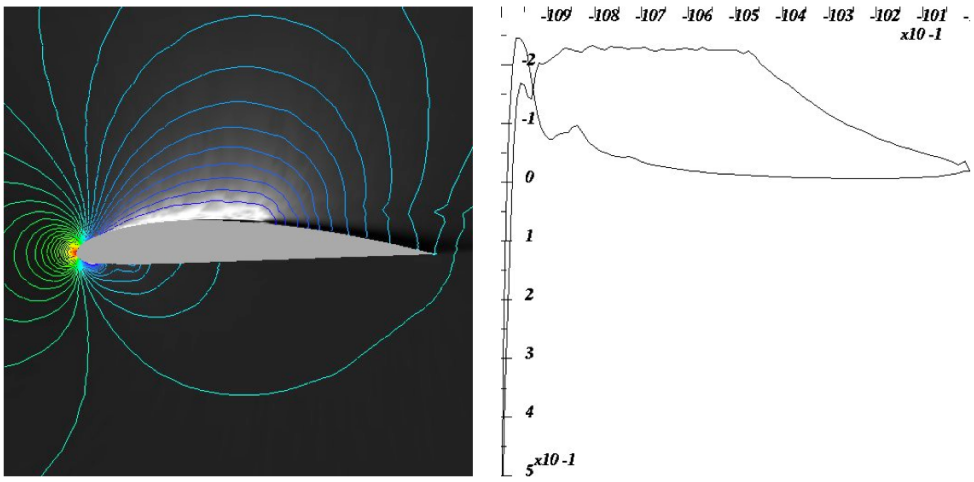

Figure 5: Flow around Clark-Y 11.4%: Model 1, σ=0.4, left; pressure contour and void fraction, right; pressure distribution around the hydrofoil

of cavitation index of 0.4 -2.0 are simulated. Here the cavitation index is defined as,

$$\sigma = \frac{p_L - p_\infty}{\frac{1}{2}\rho_L u_\infty^2} \tag{11}$$

where $(\cdot)_\infty$ denotes the uniform state. For the case of $\sigma = 0.4$ with Model 1, relatively stable sheet cavitation appears over the hydrofoil as shown in Fig. 5 where the left picture shows the pressure by contour lines and void fraction in black-and-white color, and the right graph shows the pressure distribution around the hydrofoil. So-called reentrant jet just after the sheet cavitation is clearly observed. For the case of $\sigma = 0.4$ with Model 2, the flow is more unstable and cloud cavitations are released from the sheet cavitation (Fig. 6). The higher void fraction region appears with Model 2 and thus steep density gradient also appears at the interface of liquid and gas phases. This might be the reason of instability. Averaged lift coefficient versus cavitation index is shown in Fig. 7. "exp" denotes the corresponding experiment[12] and "old" denotes the previous computation[13]. The present two models show improved results in general as well as they stably give results for very low cavitation index of 0.4.

3.2 NACA23012

The second example is flow around a hydrofoil of NACA23012. The conditions are summarized in Table 2. Figure 8 shows a close-up view of the computational grid. In low cavitation index, boundary layer of upper surface becomes unstable and vortices are released repeatedly in both models. Comparing two models, the vortices with Model 2 is stronger and vortex cavitation is observed (Fig. 9). On the other hand, the vortices do not grow in Model 1 (Fig. 10). Figures 11 and 12 shows averaged lift and drag coefficients versus cavitation index comparing with experiment[14]. At high cavitation index (no

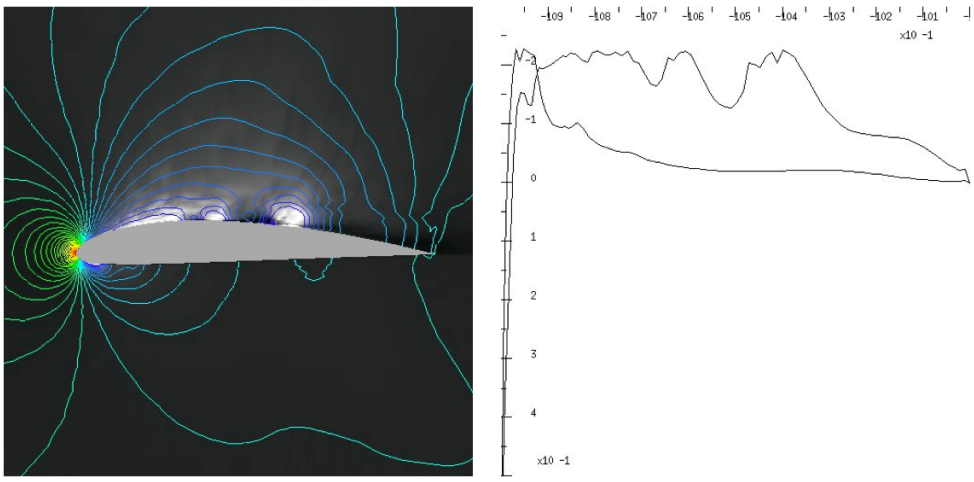

Figure 6: Flow around Clark-Y 11.4%: Model 2, σ=0.4, left; pressure contour and void fraction, right; pressure distribution around the hydrofoil

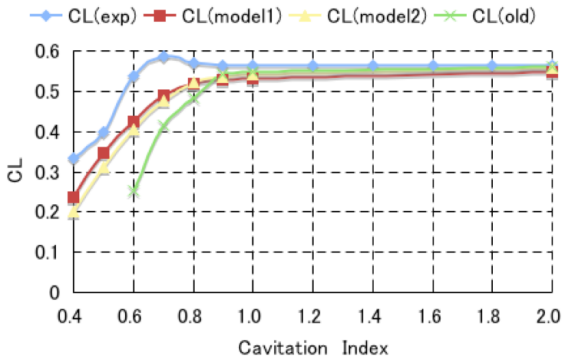

Figure 7: Lift coefficient versus cavitation index for Clark-Y 11.4%

angles-of-attack	8.0°
chord length	0.07m
initial radius of bubble nucleus	10μm
initial void fraction	0.1%
uniform flow velocity	11m/s
Reynolds number	5×10^5
surface tension	$7.2\times\ 10^{-2}$N/m
vapor pressure	2.3×10^3Pa
number of grid points	281×61

Table 2: Conditions for NACA23012

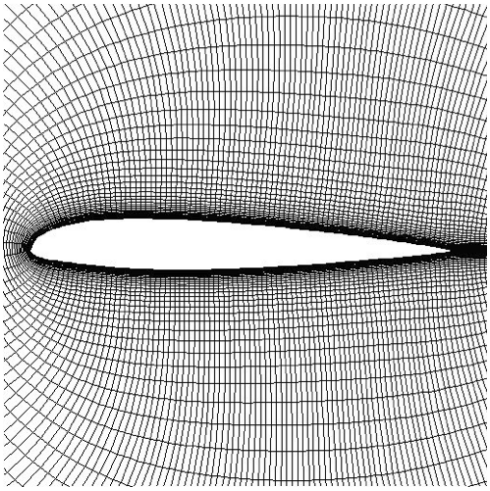

Figure 8: Computational grid for NACA23012 (close-up)

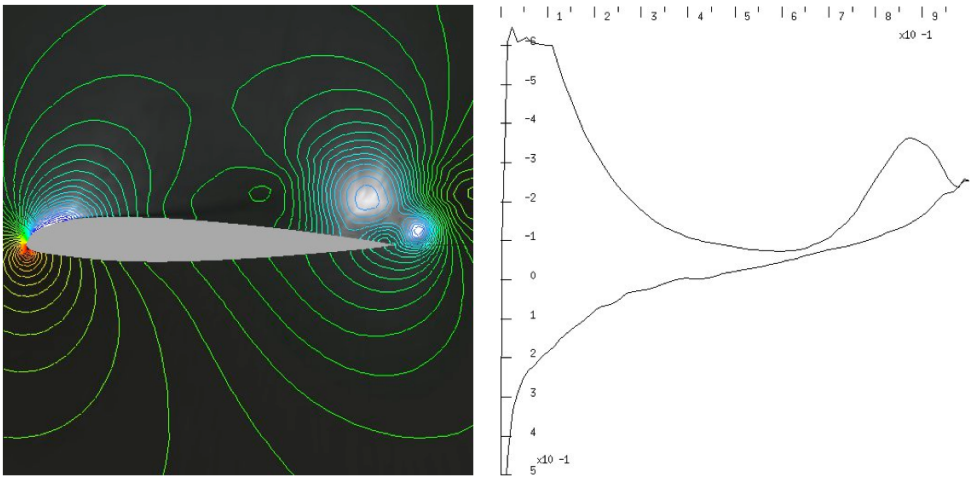

Figure 9: Flow around NACA23012: Model 2, σ=1.2, left; pressure contour and void fraction, right; pressure distribution around the hydrofoil

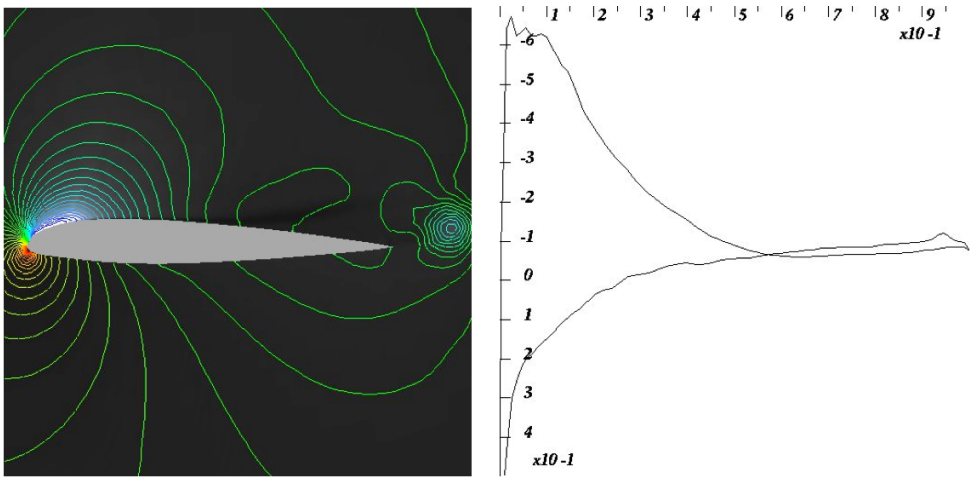

Figure 10: Flow around NACA23012: Model 1, σ=1.2, left; pressure contour and void fraction, right; pressure distribution around the hydrofoil

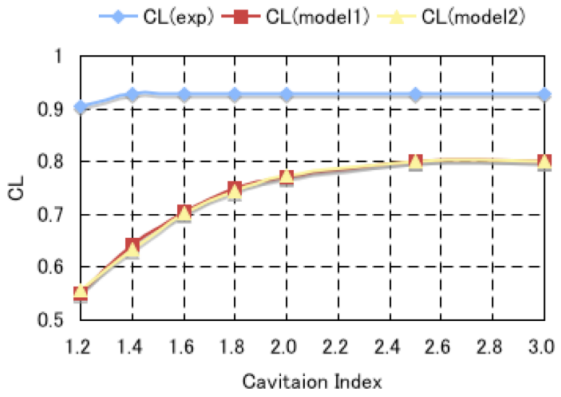

Figure 11: Lift coefficient versus cavitation index for NACA23012

cavitation / single phase case), computed results have discrepancy with experiment. This suggests that the conditions in computation and expeirment differ as no cavitation flow field must be agreed more in general. Unfortunately the experiment is old and more detailed information is difficult to obtain. However the global tendency is reproduced and very low cavitation index cases are again stably simulated.

4 CONCLUSIONS

A new bubble dynamics based cavitation model for cavitating flow simulations was proposed. The present method has advantages of bubble dynamics based model, namely, precise bubble motion and pressure. Moreover, the present method is stable in wide range of cavitation index and high void fraction can be treated. Comparison with experiment

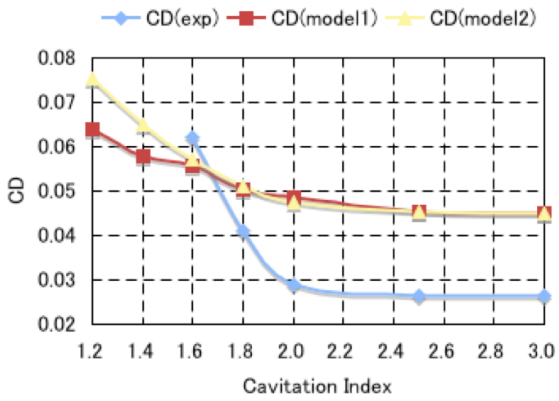

Figure 12: Drag coefficient versus cavitation index for NACA23012

showed the quantitative or qualitative agreement. For future works, the present model will be applied to the practical problems such as three-dimensional pumps[9].

REFERENCES

[1] R. F. Kunz et al., A Preconditioned Navier-Stokes Method for Two-Phase Flows with Application to Cavitation Prediction, *Computers and Fluids*, **29**, 849–875 (2000).

[2] I. Senocak and W. Shyy, A Pressure-Based Method for Turbulent Cavitating Flow Computations, *Journal of Computational Physics*, **176**, 363–383 (2002).

[3] Y. Tamura and Y. Matsumoto, Improvement of Bubble Model for Cavitating Flow Simutations, *Journal of Hydrodynamics*, **21**, 1, 41–46 (2009).

[4] N. Dumont, et al., Numerical Simulation of Cavitating Flows in Diesel Injectors by a Homogeneous Equilibrium Modeling Approach, *4th International Symposium on Cavitation* (2001).

[5] J. R. Qin, et al., Numerical Simulation of Transient External and Internal Cavitating Flows Using the Space-Time Conservation Element and Solution Element Method, ASME FEDSM'01 (2001).

[6] J. L. Reboud and Y. Delannoy, Two-Phase Flow Modelling of Unsteady Cavitation, *2nd International Symposium on Cavitation*, 39–44 (1994).

[7] B. R. Shin and T. Ikohagi, A Numerical Study of Unsteady Cavitating Flows, *3rd International Symposium on Cavitation*, 301–306 (1998).

[8] G. H. Schnerr and J. Sauer, Physical and Numerical Modeling of Unsteady Cavitation Dynamics, *4th international Conference on Multiphase Flow* (2001).

[9] M. Fukaya, Y. Tamura and Y. Matsumoto, Prediction of Cavitation Intensity and Erosion in Centrifugal Pump Based on Detailed Bubble Behavior Simulated Using Bubble Flow Model, *11th of International Symposium on Transport Phenomena and Dynamics of Rotating Machinery* (2006).

[10] F. Takemura and Y. Matsumoto, Internal Phenomena in Bubble Motion, *Bubble Dynamics and Interface Phenomena*, 467–474 (1994).

[11] Y. Tamura and Y. Matsumoto, Development and Validation of a Numerical Method for Cavitating Flow Simulation, *5th International Conference on Multiphase Flow* (2004).

[12] R. T. Knapp et al., Cavitation, Engineering Societies Monographs, McGraw-Hill, 267–320 (1970).

[13] Y. Tamura, K. Sugiyama and Y. Matsumoto, Physical Modeling and Solution Algorithm for Cavitating Flow Simulations, AIAA 2001-2652, *15th AIAA Computational Fluid Dynamics Conference* (2001).

[14] F. Numachi, Performances of Four Wing Sections with Cavitation, *Journal of Japanese Society for Mechanical Engineers*, Part 3, **7**, 28, 1–9 (1941) in Japanese.